Screen-Printed Metallization Concepts for Large-Area Back-Contact Back-Junction Silicon Solar Cells

Max Hendrichs, Milan Padilla, Johann Walter, Florian Clement, and Bernd Rech

***Abstract*—In this study, we investigate three screen-printed metallization concepts for back-contact back-junction silicon solar cells with an edge length of 156 mm: 1) a busbar-less concept with periodically interrupted contact fingers for wire-based interconnection; 2) a single-layer concept with printed busbars and periodically interrupted contact fingers; and 3) a multilayer concept consisting of continuous contact fingers, an insulation layer, and busbar metallization. A comprehensive simulation study is presented for all investigated metallization concepts, yielding their respective performance loss mechanisms. The multilayer approach is found to provide superior conversion efficiencies η, compared with the single-layer approach. For the wire-based concept, we show that contact finger interruptions up to a width of 1 mm have no significant negative impact on cell performance ($\Delta\eta < 0.1\%_{\mathrm{abs}}$). Furthermore, peel force measurements on test structures between soldered cell interconnectors and screen-printed metallization are discussed for the multilayer and the wire-based concept. Successful proof of principles with peel forces exceeding 1 N/mm are demonstrated for both investigated metallization concepts.**

***Index Terms*—Back-contact, interdigitated back contact (IBC), metallization, module integration, numerical simulation, silicon devices.**

I. Introduction

BACK-CONTACT back-junction (BC-BJ) silicon solar cells are known for their superior conversion efficiency potential both on cell [1] and module level [2]. Today, almost all commercially produced BC-BJ solar cells feature a wafer edge length of 125 mm with two rear busbars, each located at opposing wafer edges [2]. A major challenge in transferring the BC-BJ cell concept to wafers with an edge length of 156 mm is to keep resistive losses, caused by the cell metallization, on an acceptable low level. The adaption of the metallization layout with two edge busbars seems to be unsuitable for this purpose, since the contact finger length increases significantly, and thus, a higher contact finger cross-section is needed. This increased requirement can hardly be achieved with industrial screen-printing technology; hence, alternative metallization concepts have to be investigated for 156-mm BC-BJ solar cells with screen-printed contact finger metallization.

In this study, we compare three different metallization concepts for large-area BC-BJ solar cells based on screen printing that allow for low series resistance contribution of the cell metallization.

The first concept—hereinafter referred to as wire-based metallization concept—is shown in Fig. 1(a). The cell metalli-zation layout is busbar-less and is compatible with wire-based interconnection approaches such as "Multi Busbar" [3] or "SmartWire" [4]. The contact fingers feature periodic interruptions allowing for interconnecting contact fingers of each polarity by the use of wires. To the knowledge of the authors, there are no solar cell or module results published so far for this concept. The periodic contact finger interruption might result in additional resistive losses due to increased lateral current paths within the doped layers in the area of the finger interruption. Hence, the major challenge for this metallization concept is the optimization of the contact layout. On the one hand, the contact finger interruption must be wide enough to ensure a reliable cell interconnection process in an industrial-like production environment. On the other hand, it should be as small as possible in order to avoid significant cell performance losses. Within this study, we present numerical simulation results quantifying the influence of the contact finger interruption on the solar cell conversion efficiency of wire-interconnected BC-BJ solar cells.

The second concept, shown in Fig. 1(b), is referred to as single-layer metallization concept. The cell metallization consists of the contact fingers and the busbar metallization. As in case of the wire-based concept, every second contact finger is interrupted periodically, hence allowing for connecting contact fingers of each polarity with printed busbars. Due to the interruptions of the contact finger grid, the outer busbars have to be located at the wafer edges in order to collect the current of the entire solar cell area. Schinke *et al.* [5] transferred and investigated the single-layer metallization concept for BC-BJ solar cells with an edge length of 156 mm and evaporated contact finger metallization. For screen-printed BC-BJ solar cells, the major challenge for the single-layer concept is the electrical contacting property of the busbar metallization. In case a

Manuscript received August 17, 2015; revised September 21, 2015; accepted September 25, 2015. The work of M. Hendrichs was supported by the European Union's Seventh Program for research, technological development, and demonstration under Grant 608498 (project "Hercules") and by the German Federal Ministry for Economic Affairs and Energy under Contract 0325491 (project "Thesso").

M. Hendrichs is with the Fraunhofer Institute for Solar Energy Systems, Freiburg 79110, Germany, and also with Helmholtz-Zentrum Berlin, Berlin 14109, Germany (e-mail: max-sebastian.hendrichs@ise.fraunhofer.de).

M. Padilla is with the Fraunhofer Institute for Solar Energy Systems, Freiburg 79110, Germany, and also with SolarCity Corporation, Fremont, CA 94538, USA (e-mail: milan.padilla@ise.fraunhofer.de).

J. Walter and F. Clement are with the Fraunhofer Institute for Solar Energy Systems, Freiburg 79110, Germany (e-mail: johann.walter@ise.fraunhofer.dew; florian.clement@ise.fraunhofer.de).

B. Rech is with the Helmholtz Center Berlin for Materials and Energy, Berlin 12489, Germany (e-mail: bernd.rech@helmholtz-berlin.de).

Color versions of one or more of the figures in this paper are available online at http://ieeexplore.ieee.org.

Digital Object Identifier 10.1109/JPHOTOV.2015.2484960

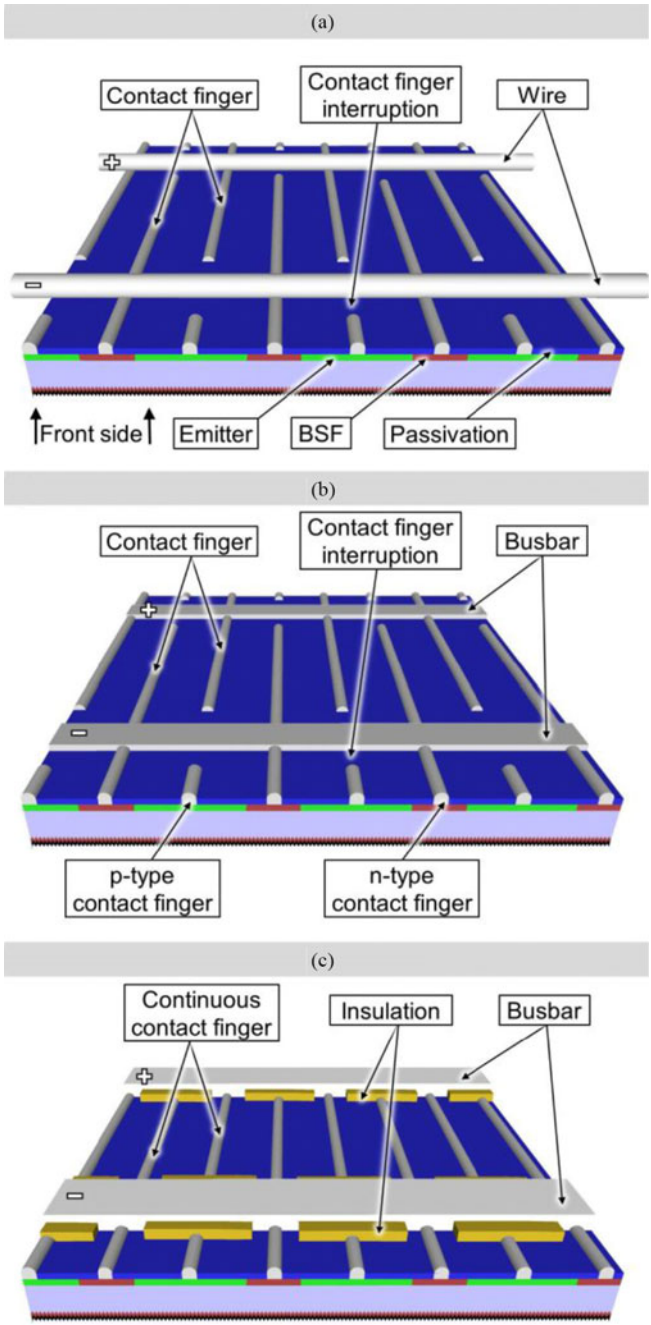

Fig. 1. Schematic cross sections of the investigated BC-BJ metallization concepts. (a) Wire-based concept, (b) single-layer concept with periodically interrupted contact fingers, and (c) multilayer concept with continuous contact fingers and intermediate insulation layer. Note that the cell front side is pointing downward.

firing-through (electrically contacting) busbar paste is applied, the doping type below the busbar must be matched with the busbar polarity. For floating (electrically noncontacting) busbar approaches, this might not be inevitably necessary. In this study, we investigate different busbar metallization setups by means of numerical simulations in order to quantify and discuss the advantages and disadvantages of different busbar configurations for this concept.

The third concept, shown in Fig. 1(c), is based on a multilayer metallization approach. The basic idea is to decouple the busbar metallization from the contact finger metallization by an intermediate insulation layer. Due to the fact that the contact fingers are not interrupted, the outer busbars are no longer necessarily located at the wafer edges, as in case of the single-layer metallization concept. The busbars might be placed flexibly within the solar cell area. This concept was introduced by Verlinden *et al.* [6] on small-area concentrator BC-BJ solar cells applying a dielectric layer stack by means of chemical vapor deposition as insulating material. Later results show that this concept is also feasible with screen-printing technology, and that it is applicable for large-area BC-BJ solar cells [7], [8]. The concept consists of three consecutively screen-printed layers: the continuous contact finger metallization, the insulation layer, and the busbar metallization. One of the major technical challenges for this metallization concept is to ensure sufficiently high peel forces of the multilayer system. In this paper, we also present adhesion force measurements on BC-BJ test structures for various busbar geometries, different soldered cell interconnectors, and different low-temperature busbar pastes. Furthermore, the conversion efficiency potential of the multilayer concept is quantified and compared with the single-layer concept [see Fig. 1(b)] by means of numerical simulations.

The results presented hereinafter are based on a previous publication in [9] in conjunction with the IEEE Conference 2015 in New Orleans, LA, USA. The numerical simulation study is expanded by including the investigation of the screen-printed single-layer and multilayer metallization concepts shown in Fig. 1(b) and (c). In case of the single-layer metallization concept, three different busbar metalli-zation configurations are investigated and discussed. Further-more, the experimental adhesion force measurement study of the multilayer metallization is expanded by an additional test layout. Moreover, results regarding a variation of the busbar paste are also shown.

II. Numerical Simulations

The simulation of full-square n-type Czochralski-grown silicon (Cz-Si) BC-BJ solar cells with an edge length of 156 mm and different metallization concepts is carried out by means of numerical unit-cell simulations. The 3-D conductive boundary based [10] simulation tool *Quokka* by Fell [11] is used for this purpose. All relevant input parameters are listed in Table I. The input parameters for the nonmetallized solar cell precursor are based on the codiffusion BC-BJ solar cell process by Keding *et al.* [12]. For this BC-BJ concept, peak conversion efficiencies of 21.6% are demonstrated on small format with PVD metallization [13]. The dark saturation current densities of the metallized areas $j_{0\mathrm{met}}$ are taken from publications dealing with screen-printed Cz-Si H-Pattern solar cells, in which the emitter contact is realized by a firing-through silver–aluminum paste, and the back surface field (BSF) contact with a firing-through silver paste [14]–[16].

The area-weighted series resistance contribution of the lateral current flow in the contact fingers r_f of both polarities is calculated using the analytical expressions from [17]

$$r_f = \frac{2}{3} R_L \cdot L_f \cdot d_{\mathrm{UC}} \frac{p}{2}. \quad (1)$$

TABLE I
INPUT PARAMETERS FOR THE NUMERICAL UNIT CELL SIMULATION USING QUOKKA

Parameter		Value	Unit
Base resistivity	ρ_{B}	3	Ω·cm
Wafer thickness	W	180	μm
Wafer edge length	l_{cell}	156	mm
Full pitch	P	1.5	mm
Emitter width	d_{E}	1200	μm
BSF width	d_{BSF}	300	μm
Contact finger width	d_{f}	50	μm
Contact resistivity of contact fingers	ρ_{C}	3	mΩ·cm^2
Line resistivity of contact fingers	R_{L}	100	Ω/m
Dark saturation current density of the firing-through metallized emitter [13], [14]	$j_{0\mathrm{met,E}}$	1500	fA/cm^2
Dark saturation current density of the firing-through metallized BSF [15]	$j_{0\mathrm{met,BSF}}$	800	fA/cm^2
Emitter sheet resistance [12]	$R_{\mathrm{SH,E}}$	65	Ω/sq
BSF sheet resistance [12]	$R_{\mathrm{SH,BSF}}$	40	Ω/sq
FSF sheet resistance [12]	$R_{\mathrm{SH,FSF}}$	235	Ω/sq
Emitter dark saturation current density [12]	$j_{0,E}$	30	fA/cm^2
BSF dark saturation current density [12]	$j_{0,\mathrm{BSF}}$	130	fA/cm^2
FSF dark saturation current density [12]	$j_{0,\mathrm{FSF}}$	43	fA/cm^2
Only for wire-based concept [see Fig. 1(a)]:			
Specific wire resistivity [17]	ρ_{wire}	5	μΩ·cm
Radius of wires	r_{wire}	125	μm
Only for busbar-based concepts [see Fig. 1(b) and (c)]:			
Specific busbar resistivity	ρ_{BB}	3	μΩ·cm
Height of busbar metallization	h_{BB}	20	μm
Number of contact pins per busbar	n_{Pin}	10	-

with R_L being the electrical line resistivity of the contact finger metallization, L_f the effective contact finger length, d_{UC} the width of the unit cell, and p the full pitch of the solar cell metallization concepts.

In case of the wire-based concept, the area-weighted series resistance of the wires r_{wire} is calculated according to [18] via

$$r_{\mathrm{wire}} = \frac{2}{3}\rho_{\mathrm{wire}}\frac{l_{\mathrm{cell}}^2 \cdot d_{\mathrm{UC}}}{\pi \cdot r_{\mathrm{wire}}^2}. \tag{2}$$

with ρ_{wire} being the specific electrical resistivity of the copper wires, l_{cell} the cell edge length, and r_{wire} the radius of the copper wires.

For the investigated busbar-based concepts, the area-weighted series resistance of the busbar metallization r_{BB} is given by [17]

$$r_{\mathrm{BB}} = \frac{2}{3}\rho_{\mathrm{BB}}\frac{l_{\mathrm{cell}}^2 \cdot d_{\mathrm{UC}}}{4 \cdot n_{\mathrm{Pin}}^2 \cdot h_{\mathrm{BB}} \cdot d_{\mathrm{BB}}}. \tag{3}$$

with ρ_{BB} being the specific electrical resistivity of the busbar, n_{Pin} the number of contact pins per busbar during cell testing, h_{BB} the height of the busbar, and d_{BB} the width of the busbar.

The calculated series resistances r_f and r_{BB} or r_f and r_{wire} are added accordingly and are considered as a lumped series resistance $r_{s,\mathrm{lumped}}$ for the *Quokka* simulation.

The schematics of the unit cells for all investigated metallization concepts are shown in Fig. 2, separated in doping pattern (left column) and metallization layout (right column). The width of the unit cell d_{UC} is defined by the wafer edge length l_{cell} and the number of contact rows per polarity n_{CR}. It is important to note that d_{UC} is calculated differently for the investigated metallization concepts. In case of the metallization concepts with

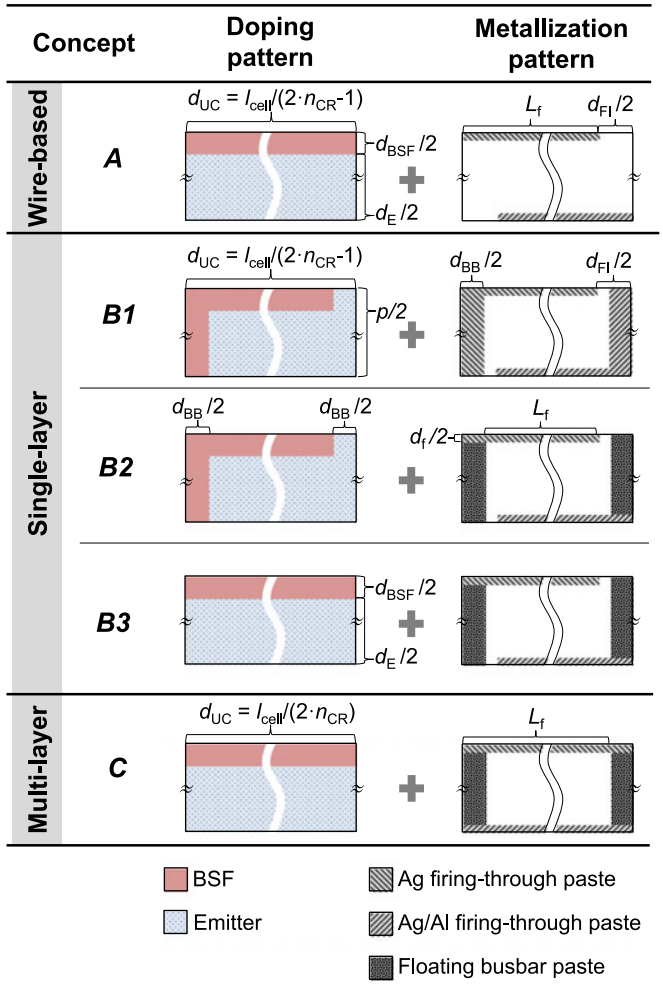

Fig. 2. Schematics of the BC-BJ unit cell in top view used for the *Quokka* simulation. Note that the view, as depicted in Fig. 1, is rotated 90°. d_{UC} is the width of the unit cell, and n_{CR} the number of contact rows per polarity, which is a sweep parameter in this simulation study.

periodic contact finger interruptions—namely the wire-based concept *A* and the single-layer concepts *B1–B3*—the width of the unit cell is calculated according to $d_{\mathrm{UC}}^{A/B} = l_{\mathrm{cell}}/(2 \cdot n_{\mathrm{CR}} - 1)$, taking into account that the outer contact rows are located at the wafer edges. In case of the multilayer concept *C*, the unit cell width is smaller, since all contact rows are evenly distributed within the solar cell area. It is calculated according to $d_{\mathrm{UC}}^{C} = l_{\mathrm{cell}}/(2 \cdot n_{\mathrm{CR}})$.

As apparent in Fig. 2, the investigated metallization concepts involve different combinations of doping and metallization patterns. The unit cell of the wire-based concept *A* features continuously doped lines below the contact finger metallization. The contact finger metallization is interrupted with a width of d_{FI}.

In case of the busbar-based single-layer metallization approach [see Fig. 1(b)], three different busbar configurations *B1–B3* are investigated. The single-layer concept *B1* is the simplest approach in terms of screen-printing process steps. In this case, the busbar metallization is realized with the same firing-through paste as the contact finger metallization, thus avoiding an additional screen-printing step for the busbar metallization. For the complete metallized area, the dark saturation current

density values $j_{0\mathrm{met},E}$ and $j_{0\mathrm{met,BSF}}$ are applied. In order to avoid electrical shuntings in the area of the busbar, the doping pattern is matched with the busbar metallization layout. Taking into account the typical alignment precision of industrial screen-printing processes [19], a safe distance between the contact fingers of one polarity and the busbar metallization of the contrary polarity is applied, $d_{\mathrm{FI}} = d_{\mathrm{BB}} + 400\ \mu$m.

In case of busbar-based single-layer concept *B2*, the floating busbar metallization is realized with a non-firing-through and noncontacting busbar paste. Compared with the single-layer concept *B1*, two additional processes are needed, namely the floating busbar printing and the curing step. As in case of concept *B1*, the doping pattern is adapted to the busbar metallization layout with the difference that the $j_{0\mathrm{met}}$ values are only applied for the areas with the firing-through contact finger metallization.

The doping pattern of the busbar-based single-layer concept *B3* consists solely of the alternating BSF and emitter areas below the contact fingers without the additionally doped areas below the busbar metallization. Like concept *B2*, the floating busbar metallization is realized in a separated screen-printing process, subsequently to the firing-through metallization of the contact fingers. Note that a practical realization of this concept is only feasible provided a noncontacting behavior of the floating busbar paste is guaranteed; otherwise, fatal shunting might occur.

The last metallization concept investigated in this simulation study is the busbar-based multilayer metallization *C* [see Fig. 1(c)]. The schematic of the unit cell appears like the unit cell of the single-layer concept *B3* with the differences that no contact finger interruption is present and the width of the unit cell d_{UC} is smaller.

A. Wire-Based Metallization Concept

In order to quantify the effect of the contact finger interruption on the current–voltage parameters of 156-mm full-square n-type Cz–Si all-screen-printed BC-BJ solar cells with wire-based metallization concept [see Fig. 1(a)], the number of contact rows per polarity $n_{\mathrm{CR}}\,(n_{\mathrm{CR}} = 10, 20, 30)$ and the width of the contact finger interruption d_{FI} ($d_{\mathrm{FI}} = 0$ mm to 3 mm) are varied systematically.

Fig. 3 shows the conversion efficiency η, open-circuit voltage V_{OC}, short-circuit current j_{SC}, fill factor *FF*, and series resistance r_{S} for the simulated wire-based n-type Cz-Si BC-BJ solar cells with different numbers of contact rows per polarity n_{CR} and different contact finger interruption widths d_{FI}. The series resistance is calculated by *Quokka* according to the double light method at the point of maximum power [20]. The highest conversion efficiency of $\eta = 21.9\%$ is found for a metallization scenario with 30 contact rows per polarity ($n_{\mathrm{CR}} = 30$) and a negligible contact finger interruption width ($d_{\mathrm{FI}} \approx 0$ mm). The conversion efficiency loss with increased d_{FI} is mainly driven by resistive losses, which result from increased lateral current paths in the nonmetallized BSF and emitter regions [21]. This main loss mechanism is reflected by the increased global series resistance r_{S}, and the corresponding drop in fill factor *FF*. Due to a decrease of the metallized area fractions and thus reduced $j_{0\mathrm{met}}$ contributions, a slight gain in V_{OC} and j_{SC} is observed

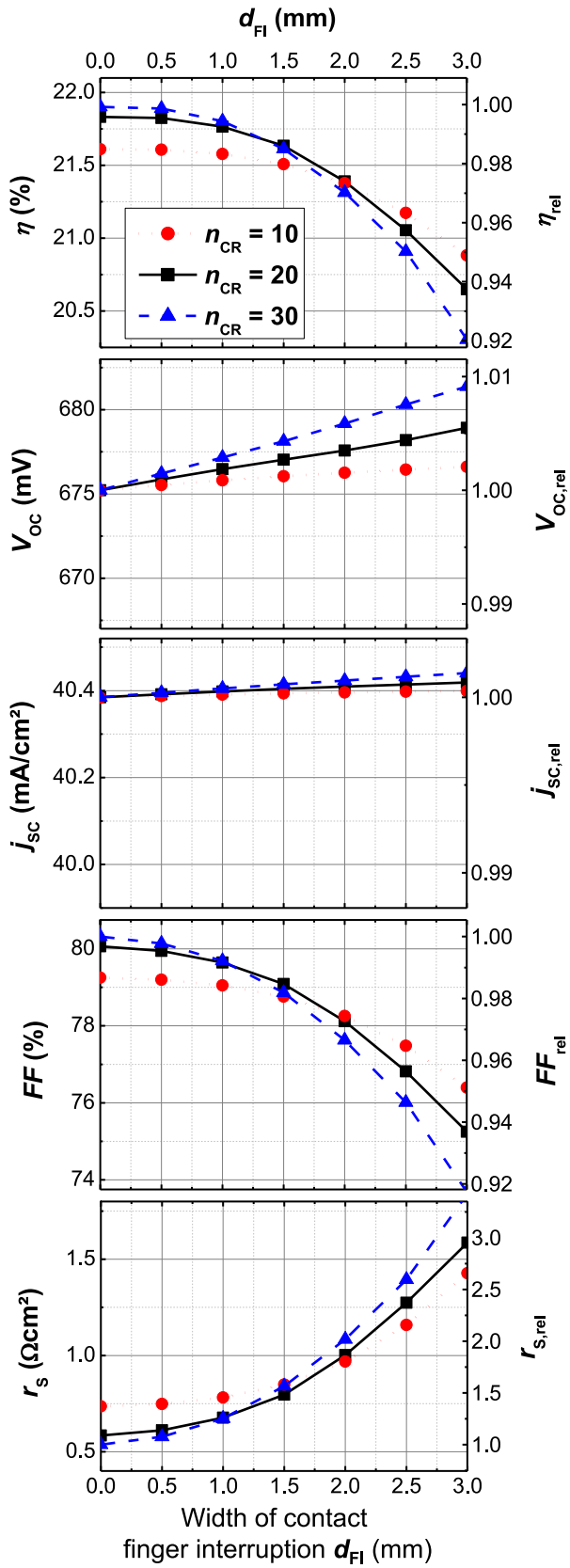

Fig. 3. Simulated solar cell parameters of n-type Cz-Si BC-J solar cells with an edge length of 156 mm and different wire-based metallization layouts [see Fig. 1(a)]. The corresponding unit cell is shown in Fig. 2 (see concept *A*). The right *y*-axis shows the parameter change relative to the idealized case with $d_{\mathrm{FI}} = 0$ mm and $n_{\mathrm{CR}} = 30$.

with increasing d_{FI}. Nevertheless, this gain is completely overcompensated by increased r_{S} losses. Metallization layouts with more contact rows per polarity n_{CR} show a sharper r_{S} raise with increasing d_{FI}, since in this case, the total number of contact finger interruptions in the cell is larger.

When it comes to the designing of the wire-based BC-BJ metallization layout, the major question is the minimum necessary contact finger interruption width suitable for a reliable interconnection process. We assume that metallization layouts with $d_{\mathrm{FI}} \approx 1$ mm are suitable for a wire-based BC-BJ interconnection process in industrial production environment. This value is considered as a conservative estimation which might be further reduced by carefully engineering of the interconnection equipment. Comparing an ideal metallization scenario without finger interruption $d_{\mathrm{FI}} = 0$ mm with metallization layouts featuring 1-mm-wide contact finger interruptions ($d_{\mathrm{FI}} = 1$ mm), the overall conversion efficiency drop is below $\Delta\eta = -0.1\%_{\mathrm{abs}}$ for all investigated numbers of contact rows per polarity n_{CR}.

B. Busbar-Based Metallization Concepts

For the busbar-based concepts with single-layer metallization (see Figs. 1(b) and 2, concepts *B1–B3*) and multilayer metallization (see Figs. 1(c) and 2, concept *C*), the influence of the busbar width d_{BB} and the number of contact rows per polarity n_{CR} on the current–voltage parameters of n-type Cz-Si BC-BJ solar cells is investigated.

Fig. 4 shows the simulated current–voltage parameters of n-type Cz-Si BC-BJ solar cells with an edge length of 156 mm and different busbar-based metallization concepts and layouts. A maximum solar cell conversion efficiency of $\eta = 22.0\%$ is calculated for the multilayer metallization concept with ten contact rows per polarity ($n_{\mathrm{CR}} = 10$). As also shown in [8], the conversion efficiency of the multilayer metallized BC-BJ solar cells increases with increasing number of contact rows per polarity. This is due to the fact that the effective contact finger length and thus the series resistance contribution of the contact finger metallization are reduced with higher numbers of contact rows per polarity. The overall superior conversion efficiency potential of the multilayer concept in comparison with the investigated single-layer concepts is based upon two reasons: First, the width of the unit cell d_{UC} is smaller, thus reducing resistive losses in the contact finger metallization. Second, additional resistive losses in the area of the contact finger interruption are absent. Switching from the multilayer approach to the single-layer concept *B3* with floating busbars, the length of the unit cell increases and the contact finger interruptions are introduced, both leading to increased resistive losses and, hence, a decreased fill factor *FF*. The next lower conversion efficiency potential is reached with the single-layer concept *B2* with adapted doping below the floating busbars. The solar cells show an additional loss mechanism, known as electrical shading [22], [23]. This effect appears in the area of the n-type busbar contacts and results in a reduction of the short-circuit current density j_{SC}. The lowest conversion efficiency potential is calculated for the simplified single-layer concept *B1* with firing-through busbar metallization. In addition to the aforementioned specific loss mechanisms of concept *B2*

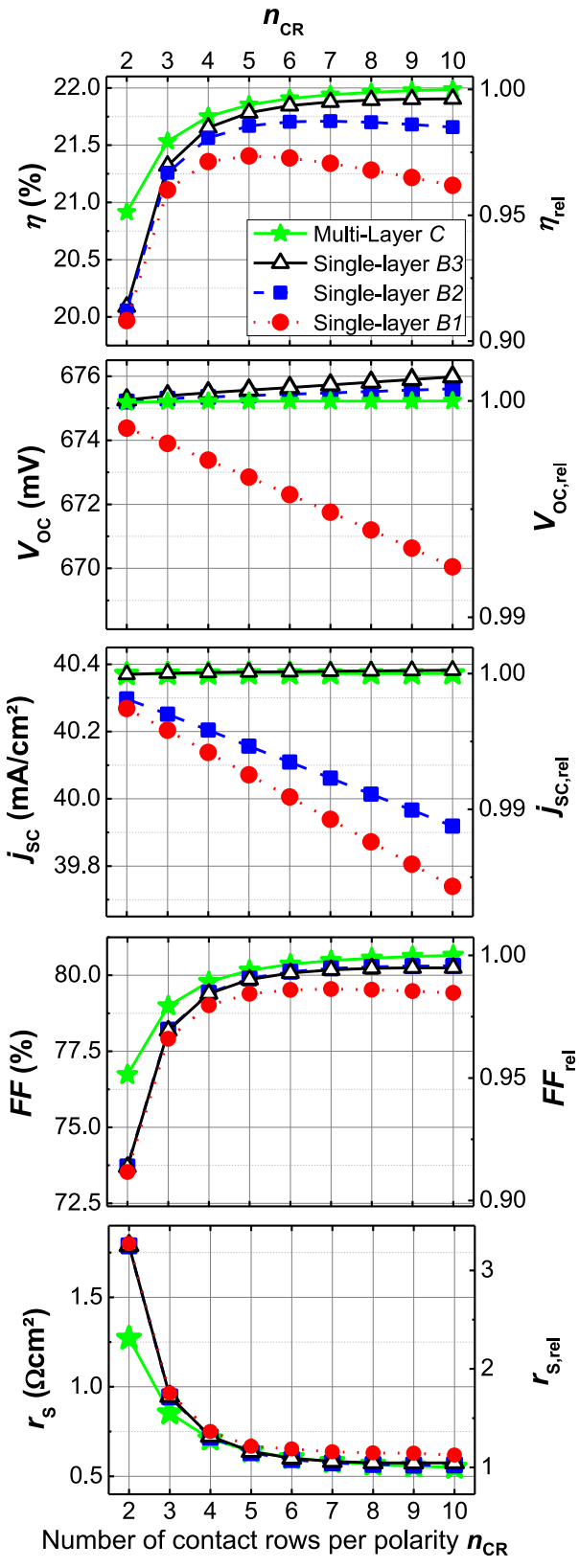

Fig. 4. Simulated solar cell parameters of n-type Cz-Si BC-BJ solar cells with an edge length of 156 mm and different busbar-based metallization layouts (see Figs. 1(b) and 2, concepts *B1–B3*, and Figs. 1(c) and 2, concept *C*, respectively). All layouts feature linear busbars with a width of $d_{\mathrm{BB}} = 1$ mm. The right y-axis is standardized to the maximum conversion efficiency value reached with a multilayer metallized solar cell with ten contact rows per polarity $n_{\mathrm{CR}} = 10$.

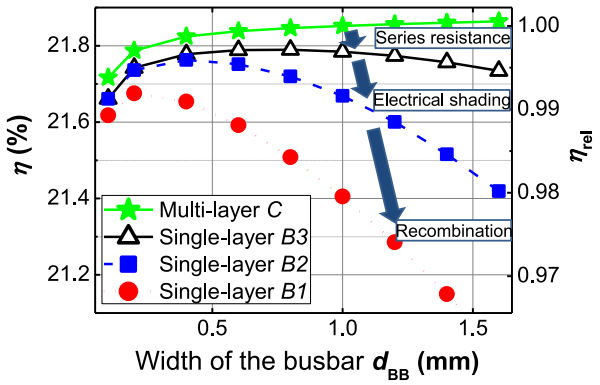

Fig. 5. Simulated solar cell conversion efficiency for varying busbar widths d_{BB} of all investigated busbar-based metallization concepts with a five-contact row metallization layout. The right y-axis is standardized to the multilayer metallization concept with 1-mm-wide busbars. The corresponding unit cells are shown in Fig. 2 concepts *B1–B3* and *C*.

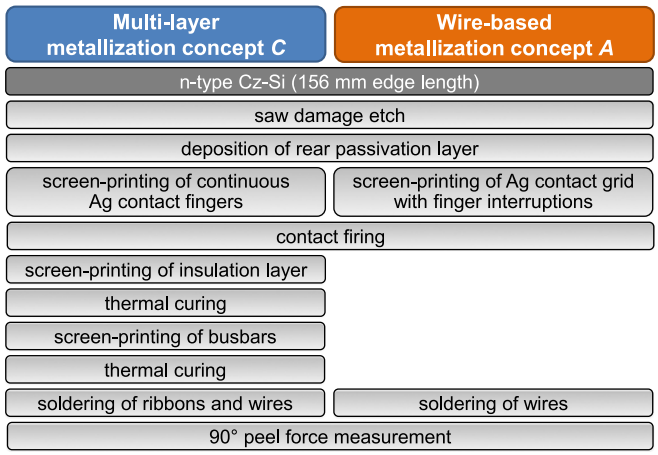

Fig. 6. Schematic process flow of the test structure fabrication for the adhesion force measurement study of different BC-BJ metallization concepts.

and *B3*, recombinative losses in the busbar-metallized areas are involved, leading to a decrease in open-circuit voltage V_{OC} and, less severely, in j_{SC}. Additionally, a reduction of the fill factor *FF* is visible especially for metallization layouts with higher numbers of contact rows n_{CR}. This loss originates on the one hand from the V_{OC} decrease and accordingly a reduction of the ideal fill factor FF_0 [24]. On the other hand, it is caused by an increased series resistance r_{S}. The additional r_{S} contribution results from the increased recombination current in the area of the firing-through busbars and, thus, a locally decreased injection level, which leads to increased internal resistive losses [25].

In our precedent work published in [8], we determined the cost optimum of multilayer metallized BC-BJ solar cells for metallization layouts with five contact rows per polarity ($n_{\mathrm{CR}} = 5$). For the present work, we take this layout as a basis for the investigation of the influence of the busbar width d_{BB} on the conversion efficiency of busbar-based metallized BC-BJ solar cells. The simulated conversion efficiency of the d_{BB} variation is shown in Fig. 5. In case of the multilayer metallization concept *C*, the conversion efficiency increases with wider busbars, since the series resistance contribution of the busbar metallization declines. Comparing the single-layer concepts *B1--B3* reveals that concept *B3* is clearly less sensitive with respect to the width of the busbars compared with concepts *B2* and *B1*. For the latter, metallization layouts with narrow busbars in the range of $d_{\mathrm{BB}} \approx 400$ μm definitely show advantages. Aiming at reduced silver consumption and maximum conversion efficiencies, we recommend applying metallization layouts with tapered busbar geometries particularly for the investigated single-layer metallization concepts *B1–B3*.

III. Peel Force Measurements

The adhesion force between soldered cell interconnectors and solar cells is investigated on metallized test structures for the wire-based metallization concept [see Fig. 1(a)] and the multilayer metallization concept [see Fig. 1(c)]. The process sequence for the fabrication of the test structures is depicted in Fig. 6. As base material, we use pseudosquare n-type Cz-Si wafers with an edge length of 156 mm, a diameter of 200 mm, and an initial thickness of 200 μm. Following alkaline saw-damage etching, an 80-nm-thick dielectric layer stack is deposited. On top, a commercial firing-through silver paste is screen-printed applying 207 contact fingers with a pitch of 750 μm, and an averaged width of 108 μm. In case of the wire-based metallization concept, the metallization grid features periodically interrupted contact fingers, whereas in case of the multilayer concept, the grid consists of continuous contact fingers. For the multilayer test structures, four additional process steps are necessary, namely the screen-printing and thermal curing of both the insulation as well as the busbar paste. As insulation material an epoxy-based solder resist and as busbar metallization, a polymer-based low-temperature paste is used. For both paste types, we apply commercially available products that are thermally cured at around 200 °C. Finally, different cell interconnectors (e.g., ribbon, wire) are soldered manually on the test structures. Identical soldering conditions are applied for each investigated interconnector group. In order to avoid cell bowing caused by the one-sided soldering, maximum three interconnectors are soldered on one sample. The peel force measurement of the cell interconnector is carried out using a Zwick tensile testing machine modified for 90°-peel testing [26].

In order to compare different interconnector dimensions, the measured peel force F is normalized to the width of the solder joint specifying the normalized peel force F_{N}. In case of soldered ribbons, the width of the solder joint is equal to the ribbon width. For the soldered wires with a diameter of $d_{\mathrm{wire}} = 270$ μm investigated in this study, a solder joint width of 330 μm is assumed.

In case of the multilayer test layouts, the average normalized peel force along the busbar metallization $\varnothing F_{\mathrm{N}}$ is calculated based on three measurement strips. In case of the wire-based test structures, the average peak peel force $\varnothing F_{\mathrm{N}}^{\mathrm{P}}$ is determined from three measurements according to [26], averaging the peel force peaks along three measurement strips. According to the current industry norm EN 50461 [27] for solar cells, the test is passed when the peel force exceeds 1 N/mm. Within this study, we apply a more specific test criterion, considering the

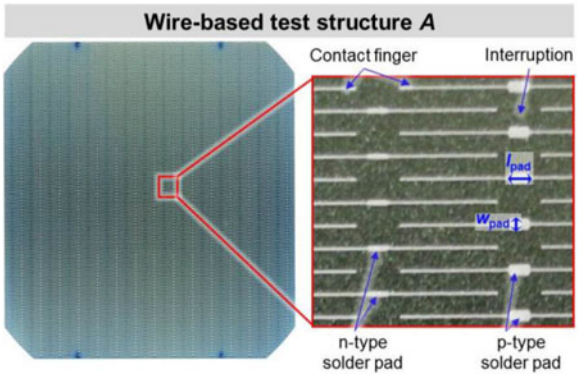

Fig. 7. Rear side of the fabricated BC-BJ test structure with wire-based metallization concept [see Fig. 1(a)] and an edge length of 156 mm before soldering of the wires.

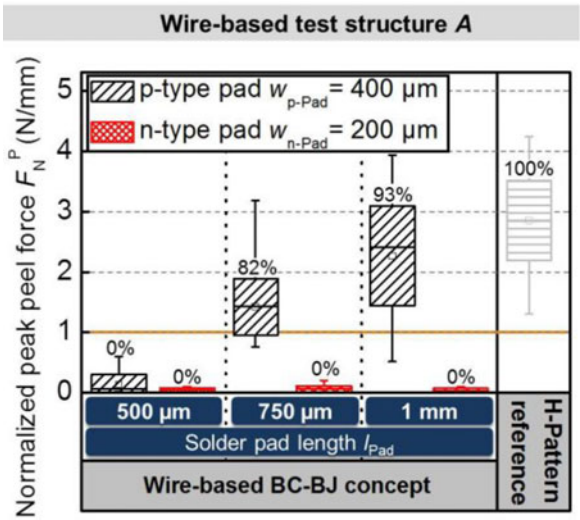

Fig. 8. Normalized peak peel force F_N^P extracted from three measurement strips of the wire-based test structures (see Fig. 7) with soldered wires ($d_{\mathrm{wire}} = 270\ \mu$m) and H-Pattern reference solar cells with 1-mm-wide copper ribbons soldered under identical conditions. The busbar geometry of the H-pattern solar cells features a metallized area of $A_{\mathrm{BB}} = 55$ mm^2 with 12 round solder pads measuring 800 μm in diameter. The relative number of peak values exceeding the 1 N/mm test criterion is specified for all groups.

test passed when >80% of the measured values is equal to or exceeds 1 N/mm.

A. Wire-Based Metallization Concept

Fig. 7 shows the silver-based metallization pattern of the fabricated BC-BJ test structures with wire-based metallization concept and an edge length of 156 mm. The layout has 15 solder pad rows per polarity ($n_{\mathrm{CR}} = 15$). Every contact finger features a small solder pad. The width of the pad is $w_{\mathrm{pad,p}} = 400\ \mu$m in case of the p-type pads and $w_{\mathrm{pad,n}} = 200\ \mu$m for the n-type pads. The pad length is varied along the wafer from $l_{\mathrm{pad}} = 0.5$ mm to $l_{\mathrm{pad}} = 1$ mm.

The results of the peel force measurement are shown in Fig. 8. The continuous line at $F_{\mathrm{N}}^{\mathrm{P}} = 1$ N/mm marks the standard threshold defined in the current industry norm [27]. The results clearly show that the pad geometry of the firing-through silver paste is a crucial parameter for the peel force of the

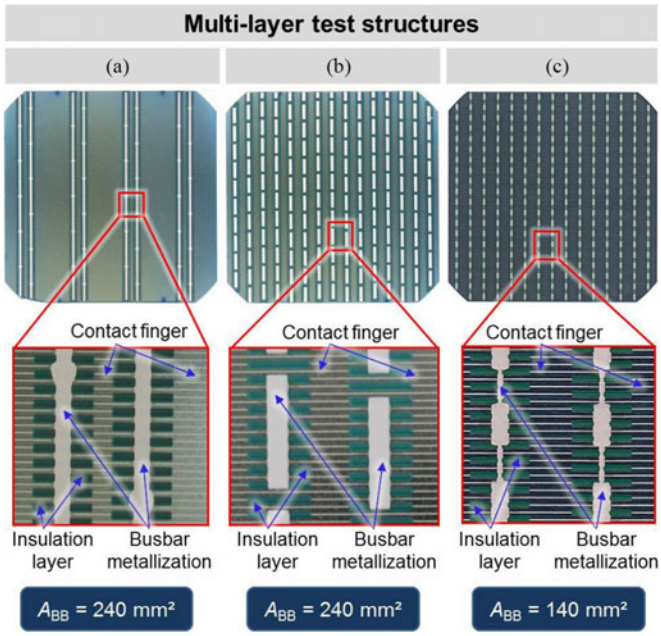

Fig. 9. Rear side of the fabricated BC-BJ test structures with busbar-based multilayer metallization [see Fig. 1(c)] and an edge length of 156 mm. (a) Group *C1*, (b) group *C2*, and (c) group *C3*. A_{BB} corresponds to the metallized area of one busbar. For group *C1*, three different low-temperature busbar pastes are examined (see Fig. 10).

wire-based metallization concept with soldered interconnectors. The width of the n-type pads $w_{\mathrm{pad,n}} = 200\ \mu$m is too small in order to achieve sufficient adhesion, resulting in peel forces well below the required 1 N/mm. In case of the wider p-type pads with $w_{\mathrm{pad,p}} = 400\ \mu$m, sufficiently high adhesion forces of $\varnothing F_{\mathrm{N}}^{\mathrm{P}} > 1$ N/mm are reached for $l_{\mathrm{pad}} \geq 0.75$ mm. The highest average normalized peak force of $\varnothing F_{\mathrm{N}}^{\mathrm{P}} = 2.3$ N/mm is achieved on solder pads with $l_{\mathrm{pad}} = 1$ mm and $w_{\mathrm{pad,p}} = 400\ \mu$m. This value is close to the peel force of an industrial three busbar H-Pattern solar cell reference for which we achieve $\varnothing F_{\mathrm{N}}^{\mathrm{P}} = 2.7$ N/mm utilizing 1-mm-wide copper ribbons. The metallization pattern of the H-Pattern cell features continuous busbars each with an area of $A_{\mathrm{BB}} = 55$ mm^2 and 12 round solder pads each measuring 800 μm in diameter. Aiming at a reduced silver consumption, a further optimization of the wire-based BC-BJ metallization design could be hybrid layout with wider pads at the solar cell edges and narrower pads within the cell area, as shown in [26] for busbar-less H-Pattern solar cells.

B. Multilayer Metallization Concept

Fig. 9 shows the three investigated metallization test layouts that are investigated for the multilayer metallization concept. Group *C1* features a layout with in total eight continuous busbars (four contact rows per polarity, $n_{\mathrm{CR}} = 4$) measuring 1.5 mm in width. Each busbar has five to six round solder pads with a diameter of 2 mm. This results in a metallized area per busbar of $A_{\mathrm{BB}} = 240$ mm^2. In order to determine the average peel force $\varnothing F_{\mathrm{N}}$, the measured peel force F_{N} is averaged along the entire busbar. In case of group *C2*, 15 discontinuous busbars are applied consisting of rectangular solder pads each with a

TABLE II
CHARACTERISTICS OF THE USED BUSBAR PASTES

Busbar paste	Particles	Silver content (WT%)	Specific resistance after curing ($\mu\Omega$·cm)
P1	Silver	90	28
P2	Silver-coated copper	10	35
P3	Copper	70	40

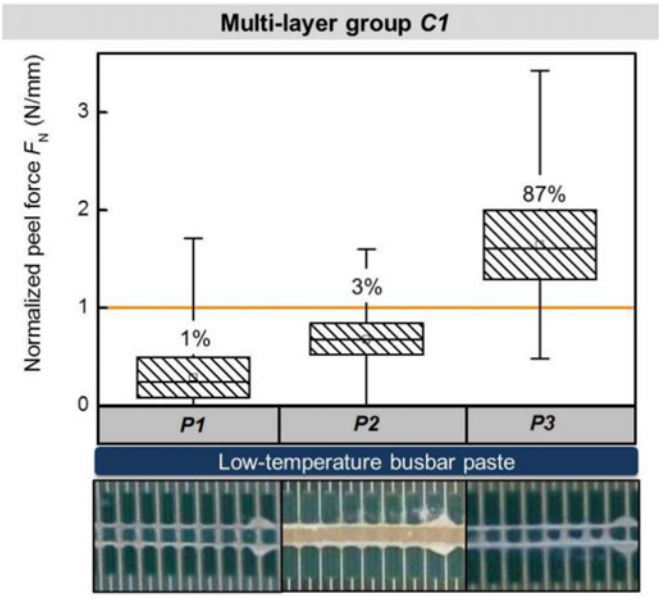

Fig. 10. Normalized peel force F_{N} between 1-mm-wide soldered ribbon and multilayer metallized BC-BJ test structures of group *C1* [see Fig. 7(a)] extracted from three peel force strips with different low-temperature busbar pastes *P1–P3*. The percentage next to the box specifies the number of values exceeding 1 N/mm. The pictures show exemplary solder pads after the peel test.

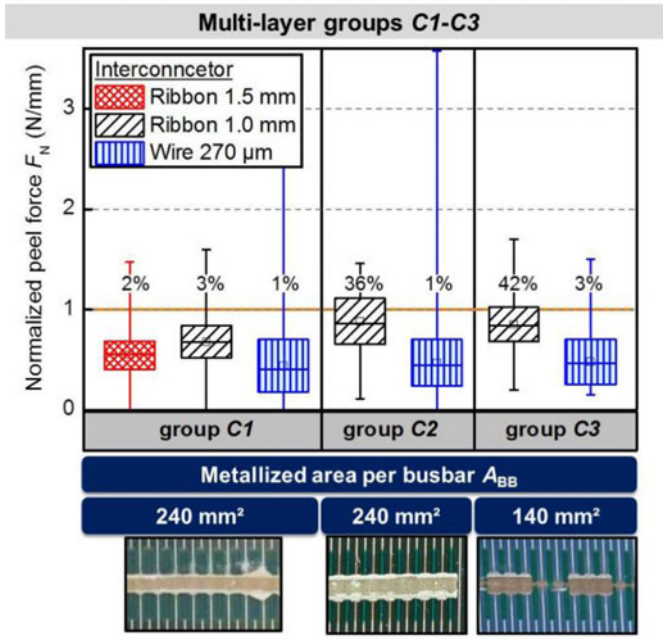

Fig. 11. Normalized peel force F_N between soldered interconnector and multilayer metallized test structures of group *C1--C3* according to Fig. 9(a)–(c) for different interconnector dimensions. All layouts are investigated with the low-temperature copper-based busbar paste *P2*. The pictures show exemplary solder pads after the peel test with 1-mm-wide ribbons.

metallized area of 2×11 mm^2, resulting in an equal metallized area per busbar of $A_{\mathrm{BB}} = 240$ mm^2. For group *C2*, only the busbar metallized sections of the peeled contact row are taken into account for the determination of $\varnothing F_{\mathrm{N}}$. The metallization layout of group *C3* features 15 contact rows each consisting of 20 rectangular solder pads with a metallized area of 1.5×4 mm^2. The solder pads are interconnected by a 300-μm-wide continuous busbar line, resulting in a reduced metallized area per busbar of $A_{\mathrm{BB}} = 140$ mm^2. The adaption of the layout allows for reducing the busbar paste consumption by $\approx 40\%$ compared with the layouts of group *C1* and *C2*. As in case of group *C2*, only the solder pad areas are considered for the calculation of $\varnothing F_{\mathrm{N}}$.

1) Influence of the Busbar Paste: First, the influence of the busbar paste on the adhesion properties is investigated. Three commercial low-temperature busbar pastes are investigated for the test layout *C1*. The investigated metallization pastes are polymer-based conductive pastes typically used for temperature-sensitive solar cell concepts as, for instance, heterojunction solar cells. Paste *P2* consists of silver-coated copper particles; pastes *P1* and *P3* are silver-based systems. Table II gives an overview of the applied busbar pastes, and Fig. 10 shows the measured normalized peel force of one exemplary peel test for 1-mm-wide Sn62Pb36Ag2 alloyed soldered copper ribbons for pastes *P1–P3*. A successful proof of principle with averaged peel forces achieving $\varnothing F_{\mathrm{N}} = 1.7$ N/mm and 87% of the measurement values exceeding $F_{\mathrm{N}} = 1$ N·m is shown with paste *P3*. The fracture after the peel force test reveals a cohesive fracture within the busbar metallization for paste *P2*. In case of the pastes *P1* and *P3*, an adhesive fracture at the interface between insulation layer and busbar metallization is visible. The significantly lower peel force of paste P1 in comparison with paste P3 is attributed to an incompatibility of the polymer components of the busbar paste with the epoxy of the solder resist.

2) Influence of the Busbar Geometry: The influence of the busbar geometry according to the test groups *C1–C3* [see Fig. 9(a)–(c)] on the peel force is analyzed for the copper-based low-temperature busbar paste *P2* and for three different soldered cell interconnectors:

1) 1-mm-wide Sn62Pb36Ag2 alloyed copper ribbon (thickness 180 μm), solder coating thickness about 18.3 μm;
2) 1.5-mm-wide Sn62Pb36Ag2 alloyed copper ribbon (thickness 150 μm), solder coating thickness about 19.0 μm;
3) Sn62Pb36Ag2 alloyed round copper wire with a diameter of 270 μm and homogenous solder coating (solder coating thickness about 10–11 μm).

The results of all groups are shown in Fig. 11. Regardless of the investigated bubsar geometry, the adhesive force of soldered wires shows low values of $\varnothing F_{\mathrm{N}} \leq 0.5$ N/mm. In case of group *C1*, the highest average adhesive force of $\varnothing F_{\mathrm{N}} = 0.7$ N/mm is reached with 1-mm-wide soldered ribbons. The analysis of

the samples after peel testing reveals a homogenous cohesive fracture in the busbar metallization. The change from continuous busbars to the pad geometry of group *C2* results in slightly higher average adhesive forces of $\varnothing F_{\mathrm{N}} = 0.9$ N/mm using a 1-mm-wide ribbon. In addition to the cohesive fracture of the busbar paste, an adhesive fracture is visible at the interface between rear passivation layer and busbar paste. The metallization layout with reduced busbar paste consumption of group *C3* shows similar results to group *C2*, revealing the potential of multilayer BC-BJ metallization layouts with reduced busbar paste consumption.

However, for all investigated groups, the weakest link of the multilayer stack is the low-temperature copper-based busbar paste. The measured average adhesive forces are fairly low compared with an industrial benchmark (a three-busbar H-Pattern solar cell with $\varnothing F_{\mathrm{N}}^{\mathrm{P}} = 2.7$ N/mm; see Fig. 8).

IV. Summary and Conclusion

Within this study, three different metallization concepts for screen-printed silicon BC-BJ solar cells with an edge length of 156 mm are investigated. The examined approaches are 1) a busbar-less concept with periodically interrupted contact fingers for wire-based interconnection; 2) a single-layer concept with busbars and periodically interrupted contact fingers; and 3) a multilayer concept consisting of continuous contact fingers, insulation layer, and busbars. First, a comprehensive simulation study is presented, yielding the individual loss mechanisms of each investigated metallization concept. Second, the multilayer and the wire-based metallization concepts are realized experimentally, aiming at specifying suitable external solder pad dimensions for solder-based interconnection approaches.

By means of numerical simulations, we quantify the impact of the periodic contact finger interruptions on the performance of screen-printed n-type Cz-Si BC-BJ solar cells. These interruptions are inevitable for the wire-based and the single-layer metallization concept and lead to additional resistive losses. According to our findings, contact finger interruption widths of up to $d_{\mathrm{FI}} = 1$ mm result in negligible conversion efficiency losses of $\Delta\eta < -0.1\%$ absolute for wire-based interconnected BC-BJ solar cells compared with an idealized scenario without contact finger interruptions. This is a very promising value, since we assume metallization layouts with $d_{\mathrm{FI}} \approx 1$ mm to be compatible with a reliable wire-based interconnection process for large-area BC-BJ solar cells. A detailed analysis of busbar-based BC-BJ concepts either with multilayer or with single-layer metallization reveals a superior conversion efficiency potential for the multilayer concept. The main advantage of the multilayer configuration is based on reduced metallization-related series resistance losses. Nevertheless, the single-layer approach offers the possibility of omitting at least one screen-printing process in the back-end manufacturing of BC-BJ solar cells, thus being ideal for low-cost BC-BJ approaches. The comparison of different single-layer-based busbar configurations reveals the individual loss mechanisms for each investigated busbar metallization scenario, such as series resistance, electrical shading, and recombination losses. The highest conversion efficiency is calculated for a floating busbar approach without adapted doping below the busbar metallization.

Furthermore, the wire-based and the multilayer me-tallization concepts are both examined experimentally on metallized BC-BJ dummies. For a variety of solder pad dimensions, the peel force with soldered interconnectors is determined. The study of different metallization designs presents important knowledge aiming at the successful transfer of the investigated concepts to functional BC-BJ solar cells with an edge length of 156 mm. In case of the wire-based concept, sufficient solder pad dimensions are found applying a pad width of 400 μm and a pad length of 0.75 mm. The measured averaged peel force amounts to 1.3 N/mm with more than 80% of the values exceeding the benchmark of $\geq$1 N/mm specified in the current industry norm. The highest averaged peel force of 2.3 N/mm is shown on 1-mm-wide solder pads, which is close to an industrial H-Pattern solar cell interconnected with 1-mm-wide ribbons. For the multilayer concept, we show that the applied low-temperature busbar paste has a crucial influence on the adhesive force of soldered ribbons. Applying an adequate paste, we reach averaged peel forces of 1.7 N/mm also passing the 80% test criterion. Discontinuous busbar geometries reveal good prospects aiming at a reduction of busbar paste consumption while maintaining sufficiently high adhesive forces. Based on the results, we present a successful proof of principle for both the multilayer and the wire-based metallization concept.

Acknowledgment

The authors would like to thank A. Fell for technical support for the *Quokka* simulations and fruitful discussions about the simulation results, S. Hoffmann and M. Retzlaff for their support during test structure manufacturing, and E. Lohmüller for proofreading the manuscript.

References

[1] K. Masuko *et al.*, "Achievement of more than 25% conversion efficiency with crystalline silicon heterojunction solar cell," *IEEE J. Photovoltaics*, vol. 4, no. 6, pp. 1433–1435, Nov. 2014.

[2] D. D. Smith *et al.*, "SunPower's maxeon gen III solar cell: High efficiency and energy yield," in *Proc. 39th IEEE Photovoltaic Spec. Conf.*, 2013, pp. 908–913.

[3] S. Braun, G. Micard, and G. Hahn, "Solar cell improvement by using a multi busbar design as front electrode," *Energy Procedia*, vol. 27, pp. 227–233, 2012.

[4] A. Schneider, L. Rubin, and G. Rubin, "Solar cell efficiency improvement by new metallization techniques—The day4 electrode concept," in *Proc. 6th IEEE World Conf.*, 2006, pp. 1095–1098.

[5] C. Schinke *et al.*, "Contacting interdigitated back-contact solar cells with four busbars for precise current–voltage measurements under standard testing conditions," *IEEE J. Photovoltaics*, vol. 2, no. 3, pp. 247–255, Jul. 2012.

[6] P. Verlinden, R. A. Sinton, and R. M. Swanson, "High efficiency large area back contact concentrator solar cells with a multilevel interconnection," *Int. J. Sol. Energy*, vol. 6, no. 6, pp. 347–366, 1988.

[7] G. Galbiati *et al.*, "Large-area back-contact back-junction solar cell with efficiency exceeding 21%," *IEEE J. Photovoltaics*, vol. 3, no. 1, pp. 560–565, Jan. 2013.

[8] M. Hendrichs, R. Keding, T. Fellmeth, A. Spribille, and F. Clement, "Optimization of multi-layer metallization design for large-area back-contact back-junction solar cells," in *Proc. 29th Eur. Photovoltaic Sol. Energy Conf. Exhib.*, 2014, pp. 412–416.

[9] M. Hendrichs *et al.*, "Evaluation of screen-printed metallization concepts for large-area back-contact back-junction solar cells," in *Proc. 42nd IEEE Photovoltaic Spec. Conf.*, 2015.

[10] R. Brendel, "Modeling solar cells with the dopant-diffused layers treated as conductive boundaries," *Prog. Photovoltaics, Res. Appl.*, vol. 20, pp. 31–43, 2010.

[11] A. Fell, K. Fong, and K. McIntosh, "3-D simulation of interdigitated-back-contact silicon solar cells with quokka including perimeter losses," *IEEE J. Photovoltaics*, vol. 4, no. 4, pp. 1040–1045, Jul. 2014.

[12] R. Keding *et al.*, "POCL3-based co-diffusion process for n-type back-contact back-junction solar cells," in *Proc. 29th Eur. Photovoltaic Sol. Energy Conf. Exhib.*, 2014, pp. 246–252.

[13] R. Keding *et al.*, "POCL3-based co-diffused process for n-type back-contact back-junction solar cells," in *Proc. 29th Eur. Photovoltaic Sol. Energy Conf. Exhib.*, 2014, pp. 677–680.

[14] A. Edler *et al.*, "Metallization-induced recombination losses of bifacial silicon solar cells," *Prog. Photovoltaics, Res. Appl.*, vol. 23, no. 5, pp. 620–627, 2015.

[15] E. Lohmüller *et al.*, "The hip-mwt+ solar cell concept on n-type silicon and metallization-induced voltage losses," in *Proc. 29th Eur. Photovoltaic Sol. Energy Conf. Exhib.*, 2014, pp. 635–641.

[16] T. Fellmeth *et al.*, "Recombination at metal-emitter interfaces of front contact technologies for highly efficient silicon solar cells," *Energy Procedia*, vol. 8, pp. 115–121, 2011.

[17] T. Fellmeth, F. Clement, and D. Biro, "Analytical modeling of industrial-related silicon solar cells," *J. Photovoltaics*, vol. 4, no. 1, pp. 504–513, 2014.

[18] S. Braun, "Simulation, analyse und herstellung von kristallinen si-solarzellen mit multi-busbar-verschaltung," Doctoral dissertation, Univ. Konstanz, Konstanz, Germany, 2014.

[19] S. Chunduri, "Raising the bar," *PHOTON Int.*, vol. 7, pp. 68–79, 2014.

[20] P. P. Altermatt *et al.*, "Spatially resolved analysis and minimization of resistive losses in high-efficiency Si solar cells," *Prog. Photovoltaics, Res. Appl.*, vol. 4, no. 6, pp. 399–414, 1996.

[21] M. Padilla *et al.*, "Local series resistance imaging of silicon solar cells with complex current paths," *IEEE J. Photovoltaics*, vol. 5, no. 3, pp. 752–758, May 2015.

[22] D. De Ceuster *et al.*, "Low cost, high volume production of $>$22% efficiency silicon solar cells," in *Proc. 22nd Eur. Photovoltaic Sol. Energy Conf. Exhib.*, 2007, pp. 816–819.

[23] M. Hermle, F. Granek, O. Schultz-Wittmann, and S. W. Glunz, "Shading effects in back-junction back-contacted silicon solar cells," in *Proc. 33rd IEEE Photovoltaic Spec. Conf.*, 2008, pp. 1–4,

[24] M. A. Green, "Accuracy of analytical expressions for solar cell fill factors," *Solar Cells*, vol. 7, pp. 337–340, 1981.

[25] J. M. Wagner, M. Hoppe, A. Schütt, H. Carstensen, and H. Föll, "Injection-level dependent series resistance: Comparison of CELLO and photoluminescence-based measurements," *Energy Procedia*, vol. 38, pp. 199–208, 2013.

[26] J. Walter, M. Tranitz, M. Volk, C. Ebert, and U. Eitner, "Multi-wire interconnection of busbar-free solar cells," *Energy Procedia*, vol. 55, pp. 380–388, 2014.

[27] *Solar Cells—Datasheet Information and Product Data for Crystalline Silicon Solar Cells*, German Version EN 50461, 2006.

Max Hendrichs was born in 1984. He studied industrial engineering and renewable energy systems in Berlin, Germany. He is currently working toward the Ph.D. degree with Fraunhofer ISE, Freiburg im Breisgau, Germany.

His research interests include innovative metallization concepts for industrial silicon based back-contact solar cells.

Milan Padilla received the Diploma degree in physics in 2011 from Technische Universität München, München, Germany, on the study of photocurrent dynamics of single GaAs nanowires. He is currently working on his dissertation with Fraunhofer ISE, Freiburg im Breisgau, Germany.

His research interests include advanced spatially resolved characterization and simulation of high-efficiency silicon solar cells using luminescence imaging and dark and illuminated lock-in thermography. His dissertation was funded by the Reiner Lemoine Stiftung.

Johann Walter received the diploma degree in electrical engineering from FH Bielefeld, Bielefeld, Germany, in 2011.

He is involved in the group Photovoltaic Modules, where he specializes in solar cell interconnection and its analyses methods. His recent publications deal with solder resists for metal wrap through Cells and multiwire interconnection.

Florian Clement studied physics with the Ludwig Maximilian University of Munich, München, Germany, and the University of Freiburg, Freiburg im Breisgau, Germany, and received the diploma degree in 2005. He received the Ph.D. degree from the University of Freiburg in 2009.

He is currently the Head of the group "MWT Solar Cells and Printing Technologies" with Fraunhofer ISE, Freiburg im Breisgau. His research interests include the development and characterization of highly efficient pilot-line-processed MWT solar cells, as well as the development and evaluation of industrial feasible thick-film technologies for solar cell metallization.

Bernd Rech received the Ph.D. degree in physics in 1997 from the RWTH Aachen, Aachen, Germany, on amorphous silicon solar cells.

He has been the Head of the Institute "Silicon Photovoltaics," Helmholtz-Zentrum Berlin, Berlin, Germany, since 2006. He is a Full Professor with the Technische Universität Berlin (chair of "photovoltaics"). Since 2008, he has been a speaker of the program "renewable energies" of the Helmholtz Association. His recent scientific work comprises crystalline silicon on glass, amorphous silicon/crystalline Si heterojunctions, and novel multijunction solar cells. He has authored and coauthored more than 300 scientific publications, as well as numerous patents.